Enhancement of the Electron−Phonon Scattering Induced by Intrinsic Surface Plasmon−Phonon Polaritons

David Hagenmüller,*,[†] Johannes Schachenmayer,[†,‡] Cyriaque Genet,[†] Thomas W. Ebbesen,[†] and Guido Pupillo*,[†,‡]

[†]ISIS (UMR 7006) and icFRC, University of Strasbourg and CNRS, Strasbourg 67081, France
[‡]IPCMS (UMR 7504), University of Strasbourg and CNRS, Strasbourg 67081, France

S *Supporting Information*

ABSTRACT: We investigate light−matter coupling in metallic crystals where plasmons coexist with phonons exhibiting large oscillator strength. We demonstrate theoretically that this coexistence can lead to strong light−matter interactions without external resonators. When the frequencies of plasmons and phonons are comparable, hybridization of these collective matter modes occurs in the crystal. We show that the coupling of these modes to photonic degrees of freedom gives rise to intrinsic surface plasmon−phonon polaritons, which offer the unique possibility to control the phonon properties by tuning the electron density and the crystal thickness. In particular, dressed phonons with reduced frequency and large wave vectors arise in the case of quasi-2D crystals, which could lead to large enhancements of the electron−phonon scattering in the vibrational ultrastrong coupling regime. This suggests that photons can play a key role in determining the quantum properties of certain materials. A nonperturbative self-consistent Hamiltonian method is presented that is valid for arbitrarily large coupling strengths.

KEYWORDS: plasmonics, polaritons, ultrastrong coupling, electron−phonon coupling, 2D materials, superconductivity
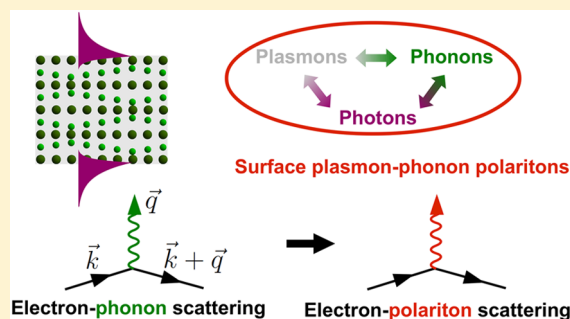
Using light to shape the properties of quantum materials is a long-standing goal in physics, which is still attracting much attention.[1−3] Since the 1960s, it is known that superconductivity can be stimulated via an amplification of the gap induced by an external electromagnetic radiation.[4,5] Ultrafast pump−probe techniques have been recently used to control the phases of materials such as magnetoresistive manganites,[6] layered high-temperature superconductors,[7] and alkali-doped fullerenes,[8] by tuning to a specific mid-infrared molecular vibration. It is an interesting question whether the phases of quantum materials may also be passively modified by strong light−matter interactions in the steady state, without external radiation. Recently, the possibility of modifying superconductivity by coupling a vibrational mode to the vacuum field of a cavity-type structure has been suggested.[9] This idea was then investigated theoretically in the case of an FeSe/SrTiO$_3$ superconducting heterostructure embedded in a Fabry−Perot cavity.[10] In this work, enhanced superconductivity relies, however, on unrealistically large values of the phonon−photon coupling strength, in a regime where light and matter degrees of freedom totally decouple.[11] This occurs beyond the ultrastrong coupling regime, which is defined when the light−matter coupling strength reaches a few tens of percents of the relevant transition frequency.[12−14]

Thanks to the confinement of light below the diffraction limit,[15] an alternative approach to engineer strong[16−26] and even ultrastrong light−matter coupling[27−29] is the use of plasmonic resonators. The latter allow the propagation of tightly confined surface plasmon polaritons (SPPs), which are evanescent waves originating from the coupling between light and collective electronic modes in metals, called plasmons.[30] Similarly, the collective coupling between light and vibrations of ions in solids gives rise to surface phonon polaritons. While suitable quantized theories to describe the ultrastrong coupling between SPPs or surface phonon polaritons and other quantum emitters such as excitons have been already reported,[31,32] most quantized models used in the literature[24,33,34] are not valid in this regime.

Strong coupling between SPPs in a 2D material and surface phonons of the substrate has stimulated considerable interest.[35−40] While significant couplings cannot generally occur in the same crystal due to the screening of the ion charges by free electrons, exceptions have been recently reported considering surface phonons in InP or SiC nanocrystals coupled to photoexcited carriers.[41] Other exceptions exist as a result of a transfer of oscillator strength from interband electronic transitions to the lattice. These include bilayer graphene,[42] alkali fullerides A$_6$C$_{60}$,[43,44] organic conductors (e.g., K−TCNQ[45−47]), and some transition metal compounds.[48] Interestingly, some of these materials or similar

compounds feature superconductivity and charge density waves under certain conditions that are believed to be driven, at least partly, by electron−phonon scattering.[49−53] Since the coexistence of collective electronic and ionic modes with large oscillator strength in the same crystal opens up the possibility to tune bulk phonon resonances,[42,54] it is interesting to ask whether strong light−matter interactions between phonons, plasmons, and photons could occur in these materials in the absence of an external resonator, and if so, can this affect the electron−phonon scattering.

In this work, we propose and investigate the possibility to tune material properties of certain crystals via a hybridization of phonons, plasmons, and photons, which is intrinsic to the material, and without the use of an external resonator. The coexistence of plasmons and phonons within the same crystal gives rise to hybrid plasmon−phonon modes, which have been extensively studied in doped semiconductors and semi-metals.[55−59] Here, we show that while hybrid plasmon−phonon modes do not affect the electron−phonon scattering at the level of the random phase approximation, strong interactions between these modes and photons offer a unique possibility to control the energy and momentum of the resulting surface plasmon−phonon polaritons by tuning the electron density and the crystal thickness: "Dressed" phonons with reduced frequency arise in the ultrastrong coupling regime, where the electronic and ionic plasma frequencies become comparable to the phonon frequency. These dressed phonons are shown to exhibit unusually large momenta comparable to the Fermi wave vector in the case of quasi-2D crystals, which could lead to large enhancements of the electron−phonon scattering. Simply put, such enhancements are significant only for thin enough crystals, as they rely on the dressing of 3D phonon modes by 2D surface polaritons. These results suggest that photons can play a key role in determining the quantum properties of certain materials.

We utilize a self-consistent Hamiltonian method based on a generalization of that introduced in ref [60], which is valid for all regimes of interactions including the ultrastrong coupling regime, and in the absence of dissipation. This quantum description of surface plasmon−phonon polaritons provides an ideal framework to investigate how the latter can affect the quantum properties of the crystal. Furthermore, our method can be generalized to various surrounding media and geometries of interest such as layered metallo-dielectric metamaterials and simple nanostructures and differs from the usual effective quantum description of strong coupling between excitons and quantized SPPs.[24,33,34] We show in the Supporting Information that the latter model leads to unphysical behaviors in the ultrastrong coupling regime.

The paper is organized as follows: (i) We first introduce the total Hamiltonian of the system under consideration and (ii) diagonalize the matter part leading to plasmon−phonon hybridization in the crystal. (iii) We derive the coupling Hamiltonian of these hybrid modes to photonic degrees of freedom, which gives rise to intrinsic surface plasmon−phonon polaritons. (iv) We determine the Hamiltonian parameter and its eigenvalues self-consistently using the Helmoltz equation and characterize the properties of the resulting surface plasmon−phonon polaritons. (v) We show that while plasmon−phonon hybridization cannot solely modify the electron−phonon scattering at the level of the random phase approximation (RPA), the coupling of these hybrid modes to

photons could lead to large enhancements of the electron−phonon scattering in the crystal.

■ QUANTUM HAMILTONIAN

We consider a metallic crystal of surface S and thickness l in air, which contains a free electron gas and a transverse optical phonon mode with frequency ω_0. The excitation spectrum of the electron gas features a collective, long-wavelength plasmon mode with plasma frequency ω_{pl}, as well as a continuum of individual excitations called electronic dark modes that are orthogonal to the plasmon mode. Both plasmons and phonons are polarized in the directions $\mathbf{u}_z$ and $\mathbf{u}_\parallel$ (Figure 1). The
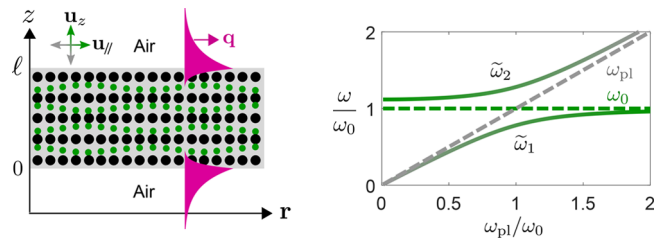

Figure 1. Intrinsic surface plasmon−phonon polaritons: Metal of thickness l in air featuring a plasmon mode with frequency ω_{pl} (gray dashed line) and an optical phonon mode with frequency ω_0 (green dashed line). Both plasmons and phonons are polarized in the directions $\mathbf{u}_z$ and $\mathbf{u}_\parallel$. When $\nu_{pn} \neq 0$ and $\omega_{pl} \approx \omega_0$, the matter Hamiltonian H_{mat} provides two hybrid plasmon−phonon modes with frequencies $\tilde{\omega}_1$ and $\tilde{\omega}_2$ [eq 1] represented as a function of ω_{pl}/ω_0 for $\nu_{pn} = 0.5\omega_0$. The surface polaritons generated by the coupling of these modes to light propagate along the two metal−dielectric interfaces with in-plane wave vector q.

Hamiltonian is derived in the Power−Zienau−Woolley representation,[61] which ensures proper inclusion of all photon-mediated dipole−dipole interactions and can be decomposed as $H = H_{pol} + H_{el−pn}$ with $H_{pol} = H_{pt} + H_{mat−pt} + H_{mat}$. The first term in H_{pol} reads $H_{pt} = \frac{1}{2\epsilon_0}\int d\mathbf{R}\mathbf{D}^2(\mathbf{R}) + \frac{1}{2\epsilon_0 c^2}\int d\mathbf{R}\mathbf{H}^2(\mathbf{R})$ and corresponds to the photon Hamiltonian. c denotes the speed of light in vacuum, $\mathbf{R} \equiv (\mathbf{r}, z)$ the 3D position, ϵ_0 is the vacuum permittivity, and $\mathbf{D}$ and $\mathbf{H}$ are the displacement and magnetic fields, respectively. The light−matter coupling term reads $H_{mat−pt} = -\frac{1}{\epsilon_0}\int d\mathbf{R}\mathbf{P}(\mathbf{R})\cdot\mathbf{D}(\mathbf{R})$. Here, $\mathbf{P} = \mathbf{P}_{pl} + \mathbf{P}_{pn}$ denotes the matter polarization field associated with the dipole moment density, where $\mathbf{P}_{pl}$ and $\mathbf{P}_{pn}$ correspond respectively to the plasmon and phonon contributions. [Our method can be easily generalized when phonons are replaced by excitons, by considering the appropriate polarization field.] The matter Hamiltonian is decomposed as $H_{mat} = H_{pn} + H_{pl} + H_{P^2}$, where H_{pn} and H_{pl} denote the contributions of free phonons and plasmons, which are provided in the Supporting Information, and $H_{P^2} = \frac{1}{2\epsilon_0}\int d\mathbf{R}\mathbf{P}^2(\mathbf{R})$ contains terms $\propto \mathbf{P}_{pl}^2$, $\mathbf{P}_{ph}^2$, and a direct plasmon−phonon interaction $\propto\mathbf{P}_{pl}\cdot\mathbf{P}_{ph}$. Finally, $H_{el−pn}$ includes the contribution of the free, individual electrons (electronic dark modes), as well as the coupling Hamiltonian between electronic dark modes and phonons.

■ DIAGONALIZATION OF THE MATTER HAMILTONIAN

Hybrid plasmon−phonon modes have been extensively studied in doped semiconductors and semimetals.[55−59] In this section,

we propose a derivation of these hybrid modes using a nonperturbative quantum method. In order to diagonalize H_{mat}, the phonon polarization $\mathbf{P}_{pn}$ is written in terms of the bosonic phonon annihilation and creation operators $B_{\mathbf{Q},\alpha}$ and $B_{\mathbf{Q},\alpha}^{\dagger}$, with the 3D wave vector $\mathbf{Q} \equiv (\mathbf{q}, q_z)$ and $\alpha = \parallel, z$ the polarization index. The lattice polarization field $\mathbf{P}_{pn}$ is proportional to the ion plasma frequency $\nu_{pn} = \sqrt{\frac{\mathcal{Z}^2 N}{M\epsilon_0 a^3}}$, which plays the role of the phonon−photon coupling strength.[62] Here, N denotes the number of vibrating ions with effective mass M and charge $\mathcal{Z}$ in a unit cell of volume a^3. The plasmon polarization $\mathbf{P}_{pl}$ is provided by the dipolar description of the free electron gas corresponding to that of the RPA.[60] In the long-wavelength regime, $\mathbf{P}_{pl}$ is written in terms of the bosonic plasmon operators $P_{\mathbf{KQ}}$ and $P_{\mathbf{KQ}}^{\dagger}$ ($\mathbf{K}$ denotes the 3D electron wave vector), superpositions of electron−hole excitations with wave vector $\mathbf{Q}$ across the Fermi surface. As explained in the Supporting Information, H_{mat} can be put in the diagonal form $H_{mat} = \sum_{\mathbf{Q},\alpha,j=1,2} \hbar\tilde{\omega}_j \Pi_{\mathbf{Q}j\alpha}^{\dagger} \Pi_{\mathbf{Q}j\alpha}$, where the hybrid plasmon−phonon operators $\Pi_{\mathbf{Q}j\alpha}$ are superpositions of $B_{\mathbf{Q},\alpha}$, $P_{\mathbf{KQ}}$, and their Hermitian conjugates, and satisfy the bosonic commutation relations $[\Pi_{\mathbf{Q}j\alpha}, \Pi_{\mathbf{Q}'j'\alpha'}^{\dagger}] = \delta_{\mathbf{Q},\mathbf{Q}'}\delta_{j,j'}\delta_{\alpha,\alpha'}$. The hybrid mode frequencies $\tilde{\omega}_j$ are represented in Figure 1 and are given by

$$2\tilde{\omega}_j^2 = \tilde{\omega}_0^2 + \omega_{pl}^2 \pm \sqrt{(\tilde{\omega}_0^2 - \omega_{pl}^2)^2 + 4\nu_{pn}^2\omega_{pl}^2} \qquad (1)$$

Here, $j = 1$ and $j = 2$ refer respectively to the signs − and +, and the longitudinal phonon mode with frequency $\tilde{\omega}_0 = \sqrt{\omega_0^2 + \nu_{pn}^2}$ is determined by the combination of the short-range restoring force related to the transverse phonon resonance, and the long-range Coulomb force associated with the ion plasma frequency. The diagonalization procedure of H_{mat} further provides the well-known transverse dielectric function of the crystal:[55]

$$\epsilon_{cr}(\omega) = 1 - \frac{\omega_{pl}^2}{\omega^2} - \frac{\nu_{pn}^2}{\omega^2 - \omega_0^2} \qquad (2)$$

One can then use the eigenmodes basis of the matter Hamiltonian to express the total polarization field as

$$\mathbf{P}(\mathbf{R}) = \sum_{\mathbf{Q},\alpha,j} g_j \sqrt{\frac{\hbar\epsilon_0\omega_{pl}^2}{2\tilde{\omega}_j V}} (\Pi_{-\mathbf{Q}j\alpha} + \Pi_{\mathbf{Q}j\alpha}^{\dagger}) e^{-i\mathbf{Q}\cdot\mathbf{R}}\mathbf{u}_{\alpha} \qquad (3)$$

with

$$g_j = \frac{\tilde{\omega}_j^2(1 + \nu_{pn}^2/\omega_{pl}^2) - \omega_0^2}{\tilde{\omega}_j^2 - \tilde{\omega}_{j'}^2} \sqrt{\frac{\omega_{pl}^4}{\tilde{\omega}_j^4} + \frac{\nu_{pn}^2\omega_{pl}^2}{(\tilde{\omega}_j^2 - \omega_0^2)^2}}$$

$j' \neq j$, and $V = Sl$. In the absence of phonon−photon coupling ($\nu_{pn} = 0$), the two modes $j = 1, 2$ reduce to the bare phonon and plasmon. A similar situation occurs for $\nu_{pn} \neq 0$, in the case of large plasmon−phonon detunings. Both in the high $\omega_{pl} \gg \omega_0$ and low $\omega_{pl} \ll \omega_0$ electron density regimes, the hybrid modes reduce to the bare plasmon and phonon excitations, and the plasmon contribution prevails in the polarization field eq 3. As explained in the following, when the latter interacts with the photonic displacement field $\mathbf{D}$, this simply results in the formation of SPPs coexisting with bare phonons. The latter are either transverse phonons with frequency ω_0 for $\omega_{pl} \gg \omega_0$ or longitudinal phonons with frequency $\tilde{\omega}_0$ in the case $\omega_{pl} \ll$

ω_0 (Figure 1). In the following, we focus on the most interesting case occurring close to the resonance $\omega_{pl} \approx \omega_0$, where plasmon−phonon hybridization occurs.

■ COUPLING TO PHOTONS

Due to the breaking of translational invariance in the z direction, the 3D photon wave vector can be split into an in-plane and a transverse component in each media as $\mathbf{Q} = q\mathbf{u}_{\parallel} + i\gamma_n\mathbf{u}_z$, where $n = d, cr$ refers to the dielectric medium and the crystal, respectively. For a given interface lying at the height z_0, the electromagnetic field associated with surface waves decays exponentially on both sides as $e^{\pm\gamma_n(z - z_0)}$ with the (real) penetration depth γ_n. The displacement and magnetic fields can be written as superpositions of the fields generated by each interfaces $m = 1, 2$, namely,

$$\mathbf{D}(\mathbf{R}) = \sum_{\mathbf{q},m} \sqrt{\frac{4\epsilon_0\hbar c}{S}} e^{i\mathbf{q}\cdot\mathbf{r}}\mathbf{u}_{\mathbf{q}m}(z)D_{\mathbf{q}m}$$

and

$$\mathbf{H}(\mathbf{R}) = \sum_{\mathbf{q},m} w_q \sqrt{\frac{4\epsilon_0\hbar c}{S}} e^{i\mathbf{q}\cdot\mathbf{r}}\mathbf{v}_{\mathbf{q}m}(z)H_{\mathbf{q}m}$$

with w_q the frequency of the surface waves (still undetermined) and $q \equiv |\mathbf{q}|$. The mode profile functions $\mathbf{u}_{\mathbf{q}m}(z)$ and $\mathbf{v}_{\mathbf{q}m}(z)$ depending on γ_n are provided in the Supporting Information. Using these expressions, the photon Hamiltonian takes the form

$$H_{pt} = \hbar c \sum_{\mathbf{q},m,m'} (\mathcal{A}_q^{mm'}D_{\mathbf{q}m}D_{-\mathbf{q}m'} + \mathcal{B}_q^{mm'}H_{\mathbf{q}m}H_{-\mathbf{q}m'})$$

where the overlap matrix elements $\mathcal{A}_q^{mm'}$ and $\mathcal{B}_q^{mm'}$ depend on the parameters γ_{cr} and γ_d. The next step corresponds to finding the electromagnetic field eigenmodes, which consist of a symmetric and an antisymmetric mode, such that the photon Hamiltonian can be put in the diagonal form:

$$H_{pt} = \hbar c \sum_{\mathbf{q},\sigma=\pm} (\alpha_{q\sigma}D_{\mathbf{q}\sigma}D_{-\mathbf{q}\sigma} + \beta_{q\sigma}H_{\mathbf{q}\sigma}H_{-\mathbf{q}\sigma})$$

with $\alpha_{q\pm} = \mathcal{A}_q^{11} \pm \mathcal{A}_q^{12}$, $\beta_{q\pm} = \mathcal{B}_q^{11} \pm \mathcal{B}_q^{12}$, $D_{\mathbf{q}\pm} = (D_{\mathbf{q}2} \pm D_{\mathbf{q}1})/\sqrt{2}$, and a similar expression for $H_{\mathbf{q}\pm}$. The new field operators $D_{\mathbf{q}\sigma}$ and $H_{\mathbf{q}\sigma}$ satisfy the commutation relations $[D_{\mathbf{q}\sigma}, H_{\mathbf{q}'\sigma'}^{\dagger}] = -iC_{q\sigma}\delta_{\mathbf{q},\mathbf{q}'}\delta_{\sigma,\sigma'}$, together with the properties $D_{\mathbf{q}\sigma}^{\dagger} = D_{-\mathbf{q}\sigma}$ and $H_{\mathbf{q}\sigma}^{\dagger} = H_{-\mathbf{q}\sigma}$. The constant $C_{q\sigma}$ is determined using the Ampère's circuital law, which provides $C_{q\sigma} = \frac{w_q}{2c\beta_{q\sigma}}$.[60]

The light−matter coupling Hamiltonian H_{mat-pt} is derived using the expression of $\mathbf{D}(\mathbf{R})$ in the new basis together with eq 3. While $\mathbf{q}$ is a good quantum number due to the in-plane translational invariance, the perpendicular wave vector of the 3D matter modes q_z is not. In the light−matter coupling Hamiltonian H_{mat-pt}, photon modes with a given $\mathbf{q}$ interact with linear superpositions of the 3D matter modes exhibiting different q_z. The latter are denoted as quasi-2D "bright" modes and are defined as $\pi_{\mathbf{q}\sigma j} = \sum_{q_z,\alpha} f_{\alpha\sigma}(Q)\Pi_{\mathbf{Q}j\alpha}$, where $f_{\alpha\sigma}(Q)$ stem from the overlap between the displacement and the polarization fields and is determined by imposing the commutation relations $[\pi_{\mathbf{q}\sigma j}, \pi_{\mathbf{q}'\sigma'j'}^{\dagger}] = \delta_{\mathbf{q},\mathbf{q}'}\delta_{\sigma,\sigma'}\delta_{j,j'}$.
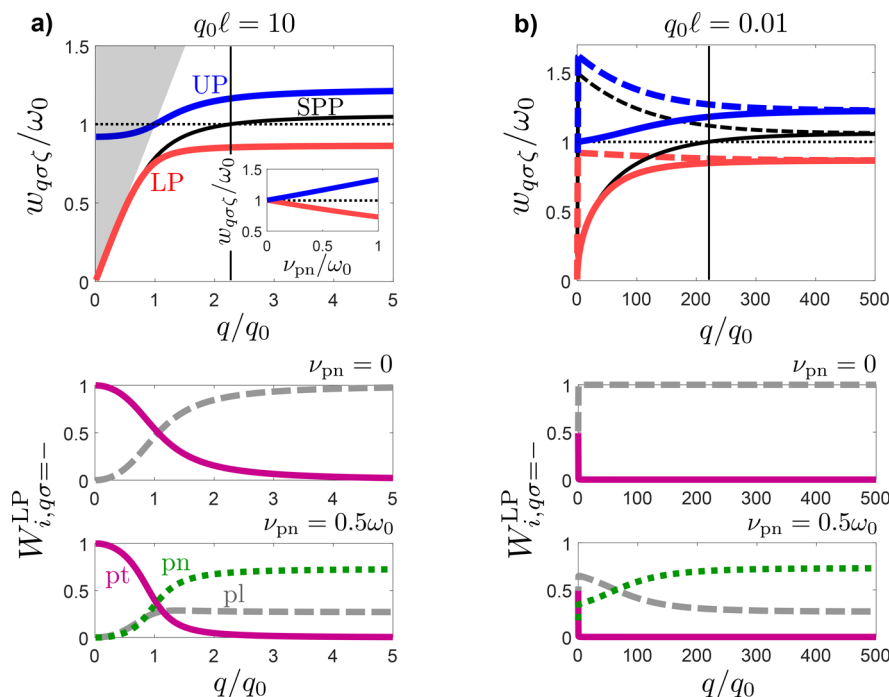
Figure 2. Normalized frequency dispersion $w_{q\sigma\zeta}/\omega_0$ and mode admixtures of the surface polaritons as a function of q/q_0 for $\omega_{pl} = 1.5\omega_0$. (a) $q_0 l = 10$. (b) $q_0 l = 0.01$. Top panels: The SPPs obtained for $\nu_{pn} = 0$ are depicted as black lines, while the surface lower and upper polaritons obtained for $\nu_{pn} = 0.5\omega_0$ are represented as thick red and blue lines, respectively. Resonance between SPPs and phonons (horizontal dotted lines) is indicated by thin vertical lines. The antisymmetric ($\sigma = -$) and symmetric ($\sigma = +$) modes correspond to the solid and dashed lines, and the light cone with boundary $\omega = qc$ is represented as a gray-shaded region. Inset: Frequency $w_{q\sigma\zeta}/\omega_0$ of the lower (red line) and upper (blue line) surface polaritons versus ν_{pn}/ω_0 for $q_0 l = 10$ and $\omega_{pl} = 1.5\omega_0$. The phonon frequency is depicted as a horizontal dotted line. Bottom panels: Plasmon (gray dashed lines), photon (magenta solid lines), and phonon (green dotted lines) admixtures of the antisymmetric lower polariton $W_{i,q\sigma = -}^{LP}$ ($i =$ pl, pt, pn) as a function of q/q_0 for $\omega_{pl} = 1.5\omega_0$. The top and bottom subpanels correspond to $\nu_{pn} = 0$ and $\nu_{pn} = 0.5\omega_0$, respectively.

Using a unitary transformation,[62] the matter Hamiltonian can be decomposed as $H_{mat} = \sum_{q,\sigma,j} \hbar\tilde{\omega}_j \pi_{q\sigma j}^\dagger \pi_{q\sigma j} + H_{dark}$, where the second term is the contribution of the "dark" modes that are orthogonal to the bright ones and which *do not interact with photons*. Without this contribution, the polariton Hamiltonian reads $H_{pol} = \sum_{q,\sigma} \mathcal{H}_{q\sigma}$ with

$$\mathcal{H}_{q\sigma} = \hbar c(\alpha_{q\sigma} D_{q\sigma} D_{-q\sigma} + \beta_{q\sigma} H_{q\sigma} H_{-q\sigma}) + \sum_j \hbar\tilde{\omega}_j \pi_{q\sigma j}^\dagger \pi_{q\sigma j}$$

$$- \sum_j \hbar\Omega_{q\sigma j}(\pi_{-q\sigma j} + \pi_{q\sigma j}^\dagger)D_{q\sigma}$$

and the vacuum Rabi frequency

$$\Omega_{q\sigma j} = g_j \sqrt{\frac{c\omega_{pl}^2}{\tilde{\omega}_j}}$$

$$\times \sqrt{\frac{q^2 + \gamma_{cr}^2}{\gamma_{cr}}(1 - e^{-2\gamma_{cr} l}) + 2l\sigma e^{-\gamma_{cr} l}(q^2 - \gamma_{cr}^2)}$$

■ SURFACE PLASMON–PHONON POLARITONS

The Hamiltonian H_{pol} exhibits three eigenvalues in each subspace (q, σ), and only the lowest two (referred to as lower and upper polaritons) correspond to surface modes (below the light cone). At this point, we have built a Hamiltonian theory providing a relation between the field penetration depths γ_n and the surface wave frequencies $w_{q\sigma\zeta}$, where $\zeta =$ LP, UP refers to the lower (LP) and upper (UP) polaritons. This eigenvalue

equation can be combined with the Helmholtz equation $\epsilon_n(\omega)\omega^2/c^2 = q^2 - \gamma_n^2$ in order to determine these parameters.[60] We use a self-consistent algorithm which starts with a given frequency $w_{q\sigma LP}$, then determine γ_n from the Helmholtz equation with $\epsilon_d = 1$ and $\epsilon_{cr}(w_{q\sigma LP})$ given by eq 2 and use these γ_n to compute the parameters entering the Hamiltonian H_{pol}. The latter is diagonalized numerically,[62] which allows determining the new $w_{q\sigma LP}$. The algorithm is applied independently for the symmetric ($\sigma = +$) and antisymmetric ($\sigma = -$) modes until convergence, which is ensured by the discontinuity of both light and matter fields at each interface.[60]

We now use this method to study the surface polaritons in our system. As an example, we consider the case $\omega_{pl} = 1.5\omega_0$ with different crystal thickness $q_0 l = 10$ (Figure 2a) and $q_0 l = 0.01$ (Figure 2b) and compute the surface polariton frequencies $w_{q\sigma\zeta}$ (top panels), as well as their phonon ($i =$ pn), plasmon ($i =$ pl), and photon ($i =$ pt) admixtures $W_{i,q\sigma}^{LP}$ for $\nu_{pn} = 0$ and $\nu_{pn} = 0.5\omega_0$ (bottom panels). Precise definitions of these quantities are provided in the Supporting Information, and l and q are both normalized to $q_0 = \omega_0/c$. Considering typical mid-infrared phonons with $\hbar\omega_0 = 0.2$ eV, the two dimensionless parameters $q_0 l = 10$ and $q_0 l = 0.01$ correspond to $l = 10\ \mu m$ (first case) and $l \approx 10$ nm (second case), respectively.

In the first case (Figure 2a), the two surface modes at each interface have negligible overlap, and the modes $\sigma_\pm$ therefore coincide. For $\nu_{pn} = 0$, the plasmon–photon coupling is responsible for the appearance of an SPP mode (black line) with frequency w_q^0, which enters in resonance with the phonon

D

mode at $q_r \approx 2.2q_0$. While for $q \ll q_0$ this SPP is mainly composed of light ($w_q^0 \sim qc$), it features a hybrid plasmon–photon character for $q \sim q_0$ and becomes mostly plasmon-like as w_q^0 approaches the surface plasmon frequency $\omega_{pl}/\sqrt{2}$ for $q \gg q_0$. For $\nu_{pn} \neq 0$, a splitting between the two polaritons branches (thick red and blue lines) is clearly visible, and the latter consist of a mix between phonons, plasmons, and photons in the vicinity of $q = q_0$. In the regime $q > q_0$, since the mostly phonon-like LP exhibits a $\sim25\%$ plasmon admixture, this polariton mode can be seen as a "dressed" phonon with frequency red-shifted from ω_0. Similarly, the "dressed" plasmon mode (UP) is blue-shifted from the surface mode frequency $\omega_{pl}/\sqrt{2}$ due its $\sim25\%$ phonon weight.

The frequencies of the LP (red line) and UP (blue line) at resonance are represented as a function of ν_{pn}/ω_0 in the inset. Here, the resonance is defined by the condition $w_q^0 = \omega_0$, which provides $q_r \approx 2.2q_0$. We observe that the polariton splitting $w_{q\sigma UP} - w_{q\sigma LP}$ is symmetric with respect to $w_{q\sigma\zeta} = \omega_0$ (black dotted line) for $\nu_{pn} \ll \omega_0$ and becomes slightly asymmetric in the ultrastrong coupling regime,[12] when ν_{pn} is a non-negligible fraction of ω_0. Furthermore, the splitting is found to decrease rapidly as the electronic plasma frequency ω_{pl} is increased.

In the second case $q_0 l = 0.01$ (Figure 2b), the crystal is thinner than the penetration depth γ_{cr} of the surface waves at the two interfaces, and the latter overlap. This results in two sets of modes $\sigma = \pm$ with different frequencies. For $\nu_{pn} = 0$, the symmetric and antisymmetric SPPs with frequency $w_{q\sigma=\pm}^0$ are represented as black dashed and solid lines, respectively. The resonance between the symmetric SPP and the phonon mode occurs for $q \approx q_0$, in the regime where the symmetric SPP is mostly photon-like with $w_{q\sigma=+}^0 \sim qc$. Interestingly, the resonance between the antisymmetric SPP and the phonon mode is now shifted to a large wave vector $q_r \approx 220q_0$, where the antisymmetric SPP exhibits a pure plasmonic character. For $q/q_0 \to \infty$, the two SPPs $\sigma = \pm$ converge to the surface plasmon frequency $\omega_{pl}/\sqrt{2}$. For $\nu_{pn} \neq 0$, the antisymmetric LP (thick red solid line) and UP (thick blue solid line) are split in the vicinity of the resonance $q_r \approx 220q_0$, while the symmetric polaritons (thick colored dashed lines) do not feature any anticrossing behavior for $q \sim q_0$. Similarly to that in (a), the LPs $\sigma = \pm$ can be seen as dressed phonon modes with frequencies red-shifted from ω_0 for large q due to their plasmon admixtures. Here, however, these dressed phonons can propagate with very large wave vectors comparable to the electronic Fermi wave vector.

■ ELECTRON–PHONON SCATTERING

We now show that the ability to tune the energy and wave vector of the dressed phonons can affect the electron–phonon scattering in the crystal. The coupling Hamiltonian between individual electrons (electronic dark modes) and phonons reads[62]

$$H_{el-pn} = \sum_K \hbar\xi_K c_K^\dagger c_K + \sum_{K,Q,\alpha} \hbar\mathcal{M} c_K^\dagger c_{K-Q}(B_{Q\alpha} + B_{-Q\alpha}^\dagger)$$

(4)

The Fermionic operators c_K and $c_K^\dagger$ annihilate and create an electron with wave vector K and energy $\hbar\xi_K$ ($K \equiv |K|$) relative to the Fermi energy. For simplicity, we assume a 3D spherical Fermi surface providing $\xi_K = \hbar(K^2 - K_F^2)/(2m)$, with m the electron effective mass and K_F the Fermi wave vector, and that

the coupling constant $\mathcal{M}$ does not depend on Q as shown theoretically for intramolecular phonons in certain crystals.[63] Electron–phonon interactions are usually characterized by the dimensionless coupling parameter λ, which quantifies the electron mass renormalization due to the coupling to phonons.[55] At zero temperature, λ is defined as

$$\lambda = \frac{1}{N_{3D}} \sum_K \delta(\xi_K) \Re(-\partial_\omega \bar{\Sigma}_K(\omega)|_{\omega=0})$$

where $\Re$ stands for real part, $N_{3D} = \sum_K \delta(\xi_K) = \frac{VmK_F}{2\pi^2\hbar}$ is the 3D electron density of states at the Fermi level, and $\partial_\omega\bar{\Sigma}_K(\omega)|_{\omega=0}$ denotes the frequency derivative of the retarded electron self-energy $\bar{\Sigma}_K(\omega)$ evaluated at $\omega = 0$. An equation of motion analysis[64] of the electron Green's function (GF) $\mathcal{G}_K(\tau) = -i\langle c_K(\tau) c_K^\dagger(0)\rangle$ allows to write the electron self-energy as

$$\Sigma_K(\omega) = \sum_{Q,\alpha} i|\mathcal{M}|^2 \int \frac{d\omega'}{2\pi} \mathcal{G}_{K-Q}(\omega + \omega') B_{Q\alpha}(\omega')$$

(5)

where $B_{Q\alpha}(\omega) = -i\int d\tau e^{i\omega\tau}\langle\mathcal{B}_{Q\alpha}(\tau)\mathcal{B}_{-Q\alpha}(0)\rangle$ is the phonon GF written in the frequency domain, and $\mathcal{B}_{Q\alpha} = B_{Q\alpha} + B_{-Q\alpha}^\dagger$. In the absence of phonon–photon coupling ($\nu_{pn} = 0$), there is no hybridization between phonons and plasmons, nor is there coupling to photons. Phonons therefore enter the Hamiltonian H_{pol} only in the free contribution $H_{pn} = \sum_{Q,\alpha} \hbar\omega_0 B_{Q\alpha}^\dagger B_{Q\alpha}$. In this case, the equation of motion analysis simply provides $B_{Q\alpha}(\omega) = 2\omega_0/(\omega^2 - \omega_0^2)$. Using this expression together with the noninteracting electron GF $\mathcal{G}_K^0(\omega) = 1/(\omega - \xi_K)$ in eq 5, one can compute the electron–phonon coupling parameter for $\nu_{pn} = 0$ as[62]

$$\lambda_0 = \frac{2|\mathcal{M}|^2}{N_{3D}\omega_0} \sum_K \delta(\xi_K) \sum_Q \delta(\xi_{K-Q}) = \frac{2|\mathcal{M}|^2 N_{3D}}{\omega_0}$$

In the presence of phonon–photon coupling ($\nu_{pn} \neq 0$), the phonon dynamics is governed by the Hamiltonian H_{pol}, which includes the coupling of phonons to plasmons and photons. It is therefore convenient to express the 3D phonon operators $B_{Q\alpha}$ and $B_{Q\alpha}^\dagger$ in terms of the 3D hybrid modes $\Pi_{Q\alpha j}$ and $\Pi_{Q\alpha j}^\dagger$ and then project the latter onto the quasi-2D bright and dark modes such that the electron–phonon Hamiltonian eq 4 takes the form $H_{el-pn} = \sum_K \hbar\xi_K c_K^\dagger c_K + H_{el-pn}^{(B)} + H_{el-pn}^{(D)}$. The contribution of the bright modes reads

$$H_{el-pn}^{(B)} = \sum_{K,Q} \sum_{\alpha,\sigma,j} \hbar\mathcal{M}\eta f_{\alpha\sigma}^*(Q) c_K^\dagger c_{K-Q}(\pi_{q\sigma j} + \pi_{-q\sigma j}^\dagger)$$

while the contribution $H_{el-pn}^{(D)}$ of the dark modes that do not interact with photons is given in the Supporting Information. Here, $\eta_j = \chi_j \sqrt{\frac{\omega_0/\tilde{\omega}_j}{(\omega_{pl}/\tilde{\omega}_j)^4 + \chi_j^2}}$ where $\chi_j = \frac{\nu_{pn}\omega_{pl}}{\tilde{\omega}_j^2 - \omega_0^2}$ is associated with the hybrid mode weights of the phonons. The electron self-energy due to the interaction with bright modes reads

$$\Sigma_K^{(B)}(\omega) = \sum_{Q,\alpha,\sigma,j} i\eta_j^2 |\mathcal{M}f_{\alpha\sigma}(Q)|^2 \int \frac{d\omega'}{2\pi} \mathcal{G}_{K-Q}(\omega + \omega')$$
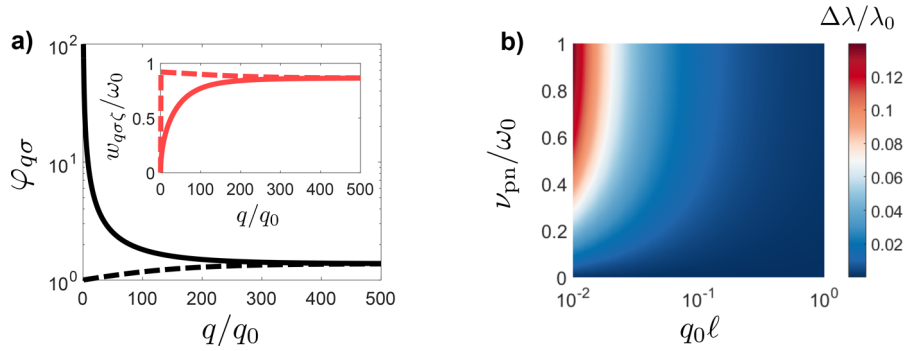$$B_{q\sigma j}(\omega')$$

(6)

Figure 3. (a) Function $\varphi_{q\sigma}$ versus q/q_0 for $\nu_{pn}/\omega_0 = 0.5$, $q_0 l = 0.01$, and $\omega_{pl} = 1.5\omega_0$. Inset: Normalized frequency dispersion of the LPs $w_{q\sigma LP}/\omega_0$ corresponding to the red solid and dashed lines in Figure 2b. The contributions of symmetric ($\sigma = +$) and antisymmetric ($\sigma = -$) modes are depicted as dashed and solid lines, respectively. (b) Relative enhancement of the electron−phonon coupling parameter $\frac{\Delta\lambda}{\lambda_0}$ given by eq 7 versus $q_0 l$ and ν_{pn}/ω_0, for $\omega_{pl} = 1.5\omega_0$ and $K_F = 10^3 q_0$.

where $\boldsymbol{B}_{q\sigma j}(\omega) = -i \int d\tau e^{i\omega\tau} \langle \Upsilon_{q\sigma j}(\tau) \Upsilon_{-q\sigma j}(0) \rangle$ and $\Upsilon_{\mathbf{q}\sigma j} = \pi_{\mathbf{q}\sigma j} + \pi^\dagger_{-\mathbf{q}\sigma j}$. As detailed in the Supporting Information, we now use the equation of motion theory to calculate the GF $\boldsymbol{B}_{q\sigma j}(\omega)$. For $\nu_{pn} = 0$, one simply obtains $\boldsymbol{B}_{q\sigma j}(\omega) = 2\tilde{\omega}_j/(\omega^2 - \tilde{\omega}_j^2)$, which provides $\boldsymbol{B}_{q\sigma 1}(\omega) = \boldsymbol{B}_{Q\alpha}(\omega)$ since $\tilde{\omega}_1 = \omega_0$ (and $\tilde{\omega}_2 = \omega_{pl}$). In this case, $\eta_1 = 1$, $\eta_2 = 0$, and only the pure phonon term $j = 1$ therefore contributes to $\Sigma_{\mathbf{K}}^{(B)}$. We then calculate $\boldsymbol{B}_{q\sigma j}(\omega)$ and the self-energy eq 6 for $\nu_{pn} \neq 0$ and decompose the electron−phonon coupling parameter into its bright and dark mode contributions: $\lambda = \lambda^{(B)} + \lambda^{(D)}$ for $\nu_{pn} \neq 0$, and $\lambda_0 = \lambda_0^{(B)} + \lambda_0^{(D)}$ for $\nu_{pn} = 0$. The contributions $\lambda^{(B)}$ and $\lambda_0^{(B)}$ are different because bright modes interact with photons for $\nu_{pn} \neq 0$, while they do not for $\nu_{pn} = 0$. Similarly, $\lambda^{(D)}$ and $\lambda_0^{(D)}$ are a priori different since dark modes are hybrid plasmon−phonon modes for $\nu_{pn} \neq 0$, while they reduce to bare phonons and plasmons for $\nu_{pn} = 0$. However, we show in the Supporting Information that $\lambda^{(D)} = \lambda_0^{(D)}$, which means that, at the level of the RPA, the hybridization between plasmons and phonons cannot solely lead to a modification of the electron−phonon scattering. Finally, the relative enhancement of the electron−phonon coupling parameter reads[62]

$$\frac{\Delta\lambda}{\lambda_0} \equiv \frac{\lambda - \lambda_0}{\lambda_0}$$
$$= \frac{1}{N_{3D}^2} \sum_{\mathbf{K}} \delta(\xi_K) \sum_{\mathbf{Q},\alpha,\sigma} (\varphi_{q\sigma} - 1)|f_{\alpha\sigma}(Q)|^2 \delta(\xi_{\mathbf{K}-\mathbf{Q}})$$

(7)

where the function $\varphi_{q\sigma}$ is given in the Supporting Information. The latter describes the renormalization of the phonon energy due to the coupling to plasmons and photons and depends on the polariton frequencies $w_{q\sigma\zeta}$. It is represented in Figure 3a together with the frequency dispersion of the LPs $w_{q\sigma LP}/\omega_0$ corresponding to the red solid and dashed lines in Figure 2b. First, we find that the contributions of the LPs to $\varphi_{q\sigma}$ largely dominate over the contributions of the other polaritons. Second, we observe that $\varphi_{q\sigma}$ is anticorrelated with the dispersion of the LPs, whenever the latter exhibit a finite phonon weight. For instance, $\varphi_{q\sigma=-}$ reaches large values in the region $q \lesssim q_0$ where the frequency of the antisymmetric LP ($\approx 35\%$ phonon for $\nu_{pn} = 0.5\omega_0$) is far away from the bare phonon frequency. In contrast, while $w_{q\sigma=+LP} \ll \omega_0$ in this region, $\varphi_{q\sigma=+} \approx 1$ since the symmetric LP is fully photon-like

for $q \lesssim q_0$. Note that for $\nu_{pn}/\omega_0 \rightarrow 0$, the LPs for $q > q_r$ are fully phonon-like with $w_{q\sigma LP} \rightarrow \omega_0$, and one finds that $\varphi_{q\sigma} \rightarrow 1$ does not contribute to $\frac{\Delta\lambda}{\lambda_0}$ in this region. For $q < q_r$, $\varphi_{q\sigma}$ does not contribute to $\frac{\Delta\lambda}{\lambda_0}$ because of the vanishing phonon weight of the LP for $\nu_{pn}/\omega_0 \rightarrow 0$.

The relative enhancement of the electron−phonon coupling $\frac{\Delta\lambda}{\lambda_0}$ is represented in Figure 3b as a function of $q_0 l$ and ν_{pn}/ω_0. We find that it can reach large values $\gtrsim 10\%$ for $\nu_{pn} \gtrsim 0.4\omega_0$ and l sufficiently small ($q_0 l \approx 0.01$). The enhancement of $\frac{\Delta\lambda}{\lambda_0}$ when decreasing the crystal thickness l can be understood by realizing that the function $|f_{\alpha\sigma}(Q)|^2$ entering eq 7 scales as $\sim 1/(\gamma_{cr} l)$, as shown in the Supporting Information. This stems from the fact that the dressing of 3D phonons by 2D evanescent waves decaying exponentially at each interface increases when decreasing the crystal thickness. However, when the crystal thickness becomes too small (e.g., when $K_F l \lesssim 1$), the description of the matter excitations by 3D fields breaks down, and quantum confinement effects have to be taken into account in the model. The parameters of Figure 3b are $l = 10$ nm for $\hbar\omega_0 = 0.2$ eV, and $K_F = 1$ nm^{-1}. We find that the enhancement of the electron−phonon coupling strongly increases with the ratio q_0/K_F, i.e., when the mismatch between the typical photonic and electronic wave vectors is reduced. This can occur in materials with larger phonon frequency and/or lower electron density. In the latter case, however, decreasing K_F requires considering larger l for the 3D description of the matter fields to be valid, which in turn leads to a reduction of $\frac{\Delta\lambda}{\lambda_0}$.

For instance, bilayer graphene with $l \approx 0.4$nm[65] exhibits an infrared-active phonon mode at $\hbar\omega_0 = 0.2$ eV[42] and has been recently shown to feature superconductivity at low carrier densities $\approx 2 \times 10^{12}$ cm^{-2} when the two sheets of graphene are twisted relative to each other by a small angle.[52] In this regime, we find that $\omega_{pl} \approx \omega_0$, $q_0 l \approx 7 \times 10^{-4}$, $K_F \approx 1.6 \times 10^3 q_0$, and the large phonon−photon coupling strengths $\nu_{pn} \approx 0.25\omega_0$[42] allow reaching the ultrastrong coupling regime. Using these parameters, we find that the contribution of surface plasmon−phonon polaritons to the electron−phonon scattering is expected to reach a very large value, $\frac{\Delta\lambda}{\lambda_0} \approx 2.7$. However, the

small thickness of bilayer graphene such that $K_F l \sim 1$ in this weakly doped regime implies that quantum confinement effects become important. Furthermore, the failure of the 3D model assuming $\omega_{pl} \to$ const as $q \to 0$ can be seen in the dispersion of the optical plasmon mode in bilayer graphene,[58] which is known to be $\omega_{pl} \sim \sqrt{q}$ as $q \to 0$.

CONCLUSION

In summary, we have carried out a nonperturbative quantum theory of intrinsic, lossless plasmon–phonon polaritons valid for arbitrary large coupling strengths and discussed the different regimes of interest obtained by tuning the crystal thickness and the phonon–photon coupling strength. This theory allows characterizing the hybridization between plasmons and phonons in the crystal, which cannot lead solely to a modification of the electron–phonon scattering at the level of the RPA. Considering the coupling of these hybrid plasmon–phonon modes to photons, we have found that in the regime where both the electronic and ionic plasma frequencies become comparable to the phonon frequency, a dressed low-energy phonon mode with finite plasmon weight arises. In the case of quasi-2D crystals, the in-plane wave vector of this dressed phonon can reach very large values comparable to the Fermi wave vector, which is shown to lead to an enhancement of the electron–phonon scattering. It is an interesting prospect to investigate whether this effect could modify superconductivity in certain molecular crystals. While our model specifically addresses the case of metallic crystals with large ionic charges supporting far/mid-infrared pho-nons,[42–45,47] it can be directly generalized to describe other types of excitations such as excitons and extended to other geometries. Further useful extensions include the presence of quantum confinement in 2D materials and dissipation. In addition to the intrinsic phonon linewidth, the main source of dissipation is the damping of plasmons with large wave vectors due to the electron–hole continuum (electronic dark modes).[55] However, since the dressed phonons feature only a ~25% plasmon admixture at large wave vectors, this effect is not expected to dramatically affect our results.

ASSOCIATED CONTENT

Ⓢ Supporting Information

The Supporting Information is available free of charge on the ACS Publications website at DOI: 10.1021/acsphoto-nics.9b00268.

> Detailed diagonalization of the matter Hamiltonian, derivation of the total Hamiltonian and diagonalization, derivation of the electron–phonon coupling Hamilto-nian, calculation of the relative change of the electron–phonon coupling parameter, derivation of the effective quantum model, figure showing the failure of the effective quantum model in the ultrastrong coupling regime (PDF)

AUTHOR INFORMATION

Corresponding Authors
*E-mail: dhagenmuller@unistra.fr.
*E-mail: pupillo@unistra.fr.
ORCID Ⓞ
David Hagenmüller: 0000-0003-4129-9312
Cyriaque Genet: 0000-0003-0672-7406
Thomas W. Ebbesen: 0000-0002-3999-1636
Notes
The authors declare no competing financial interest.

ACKNOWLEDGMENTS

REFERENCES

(1) Schlawin, F.; Cavalleri, A.; Jaksch, D. Cavity-mediated electron-photon superconductivity. *ArXiv e-prints*, **2018**.

(2) Curtis, J. B.; Raines, Z. M.; Allocca, A. A.; Hafezi, M.; Galitski, V. M. Cavity Quantum Eliashberg Enhancement of Superconductivity. *ArXiv e-prints*, **2018**.

(3) Mazza, G.; Georges, A. Superradiant Quantum Materials. *Phys. Rev. Lett.* **2019**, *122*, No. 017401.

(4) Anderson, P. W.; Dayem, A. H. Radio-Frequency Effects in Superconducting Thin Film Bridges. *Phys. Rev. Lett.* **1964**, *13*, 195–197.

(5) Wyatt, A. F. G.; Dmitriev, V. M.; Moore, W. S.; Sheard, F. W. Microwave-Enhanced Critical Supercurrents in Constricted Tin Films. *Phys. Rev. Lett.* **1966**, *16*, 1166–1169.

(6) Rini, M.; Tobey, R.; Dean, N.; Itatani, J.; Tomioka, Y.; Tokura, Y.; Schoenlein, R. W.; Cavalleri, A. Control of the electronic phase of a Manganite by mode-selective vibrational excitation. *Nature* **2007**, *449*, 72.

(7) Fausti, D.; Tobey, R. I.; Dean, N.; Kaiser, S.; Dienst, A.; Hoffmann, M. C.; Pyon, S.; Takayama, T.; Takagi, H.; Cavalleri, A. Light-Induced Superconductivity in a Stripe-Ordered Cuprate. *Science* **2011**, *331*, 189–191.

(8) Mitrano, M.; Cantaluppi, A.; Nicoletti, D.; Kaiser, S.; Perucchi, A.; Lupi, S.; Di Pietro, P.; Pontiroli, D.; Riccò, M.; Clark, S. R.; Jaksch, D.; Cavalleri, A. Possible light-induced superconductivity in K_3C_{60} at high temperature. *Nature* **2016**, *530*, 461–464.

(9) Ebbesen, T. W. Hybrid Light-Matter States in a Molecular and Material Science Perspective. *Acc. Chem. Res.* **2016**, *49*, 2403–2412.

(10) Sentef, M. A.; Ruggenthaler, M.; Rubio, A. Cavity quantum-electrodynamical polaritonically enhanced electron-phonon coupling and its influence on superconductivity. *Sci. Adv.* **2018**, *4*, eaau6969,

(11) De Liberato, S. Light-Matter Decoupling in the Deep Strong Coupling Regime: The Breakdown of the Purcell Effect. *Phys. Rev. Lett.* **2014**, *112*, No. 016401.

(12) Ciuti, C.; Bastard, G.; Carusotto, I. Quantum vacuum properties of the intersubband cavity polariton field. *Phys. Rev. B: Condens. Matter Mater. Phys.* **2005**, *72*, 115303.

(13) Forn-Díaz, P.; Lamata, L.; Rico, E.; Kono, J.; Solano, E. Ultrastrong coupling regimes of light-matter interaction. *ArXiv e-prints* 2018,.

(14) Kockum, A. F.; Miranowicz, A.; De Liberato, S.; Savasta, S.; Nori, F. Ultrastrong coupling between light and matter. *Nat. Rev. Phys.* **2019**, *1*, 19–40.

(15) Barnes, W. L.; Dereux, A.; Ebbesen, T. W. Surface plasmon subwavelength optics. *Nature* **2003**, *424*, 824.

(16) Agranovich, V.; Malshukov, A. Surface polariton spectra if the resonance with the transition layer vibrations exist. *Opt. Commun.* **1974**, *11*, 169–171.

(17) Yakovlev, V.; Nazin, V.; Zhizhin, G. The surface polariton splitting due to thin surface film LO vibrations. *Opt. Commun.* **1975**, *15*, 293–295.

(18) Pockrand, I.; Brillante, A.; Möbius, D. Exciton-surface plasmon coupling: An experimental investigation. *J. Chem. Phys.* **1982**, *77*, 6289–6295.

(19) Bellessa, J.; Bonnand, C.; Plenet, J. C.; Mugnier, J. Strong Coupling between Surface Plasmons and Excitons in an Organic Semiconductor. *Phys. Rev. Lett.* **2004**, *93*, No. 036404.

(20) Dintinger, J.; Klein, S.; Bustos, F.; Barnes, W. L.; Ebbesen, T. W. Strong coupling between surface plasmon-polaritons and organic molecules in subwavelength hole arrays. *Phys. Rev. B: Condens. Matter Mater. Phys.* **2005**, *71*, No. 035424.

(21) Vasa, P.; Pomraenke, R.; Schwieger, S.; Mazur, Y. I.; Kunets, V.; Srinivasan, P.; Johnson, E.; Kihm, J. E.; Kim, D. S.; Runge, E.; Salamo, G.; Lienau, C. Coherent Exciton-Surface-Plasmon-Polariton Inter-action in Hybrid Metal-Semiconductor Nanostructures. *Phys. Rev. Lett.* **2008**, *101*, 116801.

(22) Gómez, D. E.; Vernon, K. C.; Mulvaney, P.; Davis, T. J. Surface Plasmon Mediated Strong Exciton-Photon Coupling in Semi-conductor Nanocrystals. *Nano Lett.* **2010**, *10*, 274–278.

(23) Berrier, A.; Cools, R.; Arnold, C.; Offermans, P.; Crego-Calama, M.; Brongersma, S. H.; Gómez-Rivas, J. Active Control of the Strong Coupling Regime between Porphyrin Excitons and Surface Plasmon Polaritons. *ACS Nano* **2011**, *5*, 6226–6232.

(24) González-Tudela, A.; Huidobro, P. A.; Martín-Moreno, L.; Tejedor, C.; García-Vidal, F. J. Theory of Strong Coupling between Quantum Emitters and Propagating Surface Plasmons. *Phys. Rev. Lett.* **2013**, *110*, 126801.

(25) Orgiu, E.; George, J.; Hutchison, J.; Devaux, E.; Dayen, J. F.; Doudin, B.; Stellacci, F.; Genet, C.; Schachenmayer, J.; Genes, C.; Pupillo, G.; Samori, P.; Ebbesen, T. W. Conductivity in organic semiconductors hybridized with the vacuum field. *Nat. Mater.* **2015**, *14*, 1123–1129.

(26) Zhang, Y.; Meng, Q.-S.; Zhang, L.; Luo, Y.; Yu, Y.-J.; Yang, B.; Zhang, Y.; Esteban, R.; Aizpurua, J.; Luo, Y.; Yang, J.-L.; Dong, Z.-C.; Hou, J. G. Sub-nanometre control of the coherent interaction between a single molecule and a plasmonic nanocavity. *Nat. Commun.* **2017**, *8*, 15225.

(27) Balci, S. Ultrastrong plasmon-exciton coupling in metal nanoprisms with J-aggregates. *Opt. Lett.* **2013**, *38*, 4498–4501.

(28) Cacciola, A.; Di Stefano, O.; Stassi, R.; Saija, R.; Savasta, S. Ultrastrong Coupling of Plasmons and Excitons in a Nanoshell. *ACS Nano* **2014**, *8*, 11483–11492.

(29) Todisco, F.; De Giorgi, M.; Esposito, M.; De Marco, L.; Zizzari, A.; Bianco, M.; Dominici, L.; Ballarini, D.; Arima, V.; Gigli, G.; Sanvitto, D. Ultrastrong Plasmon-Exciton Coupling by Dynamic Molecular Aggregation. *ACS Photonics* **2018**, *5*, 143–150.

(30) Raether, H. *Surface Plasmons on Smooth and Rough Surfaces and on Gratings*; Springer-Verlag: Berlin, Heidelberg, 1988.

(31) Alpeggiani, F.; Andreani, L. C. Quantum Theory of Surface Plasmon Polaritons: Planar and Spherical Geometries. *Plasmonics* **2014**, *9*, 965–978.

(32) Gubbin, C. R.; Maier, S. A.; De Liberato, S. Real-space Hopfield diagonalization of inhomogeneous dispersive media. *Phys. Rev. B: Condens. Matter Mater. Phys.* **2016**, *94*, 205301.

(33) Hümmer, T.; García-Vidal, F. J.; Martín-Moreno, L.; Zueco, D. Weak and strong coupling regimes in plasmonic QED. *Phys. Rev. B: Condens. Matter Mater. Phys.* **2013**, *87*, 115419.

(34) Delga, A.; Feist, J.; Bravo-Abad, J.; Garcia-Vidal, F. J. Theory of strong coupling between quantum emitters and localized surface plasmons. *J. Opt.* **2014**, *16*, 114018.

(35) Koch, R. J.; Seyller, T.; Schaefer, J. A. Strong phonon-plasmon coupled modes in the graphene/silicon carbide heterosystem. *Phys. Rev. B: Condens. Matter Mater. Phys.* **2010**, *82*, 201413.

(36) Brar, V. W.; Jang, M. S.; Sherrott, M.; Kim, S.; Lopez, J. J.; Kim, L. B.; Choi, M.; Atwater, H. Hybrid Surface-Phonon-Plasmon Polariton Modes in Graphene/Monolayer h-BN Heterostructures. *Nano Lett.* **2014**, *14*, 3876–3880.

(37) Koch, R. J.; Fryska, S.; Ostler, M.; Endlich, M.; Speck, F.; Hänsel, T.; Schaefer, J. A.; Seyller, T. Robust Phonon-Plasmon Coupling in Quasifreestanding Graphene on Silicon Carbide. *Phys. Rev. Lett.* **2016**, *116*, 106802.

(38) Lin, X.; Yang, Y.; Rivera, N.; López, J. J.; Shen, Y.; Kaminer, I.; Chen, H.; Zhang, B.; Joannopoulos, J. D.; Soljačić, M. All-angle

(39) Settnes, M.; Saavedra, J. R. M.; Thygesen, K. S.; Jauho, A.-P.; García de Abajo, F. J.; Mortensen, N. A. Strong Plasmon-Phonon Splitting and Hybridization in 2D Materials Revealed through a Self-Energy Approach. *ACS Photonics* **2017**, *4*, 2908–2915.

(40) Li, K.; Fitzgerald, J. M.; Xiao, X.; Caldwell, J. D.; Zhang, C.; Maier, S. A.; Li, X.; Giannini, V. Graphene Plasmon Cavities Made with Silicon Carbide. *ACS Omega* **2017**, *2*, 3640–3646.

(41) Dunkelberger, A. D.; Ellis, C. T.; Ratchford, D. C.; Giles, A. J.; Kim, M.; Kim, C. S.; Spann, B. T.; Vurgaftman, I.; Tischler, J. G.; Long, J. P.; Glembocki, O. J.; Owrutsky, J. C.; Caldwell, J. D. Active tuning of surface phonon polariton resonances via carrier photo-injection. *Nat. Photonics* **2018**, *12*, 50–56.

(42) Kuzmenko, A. B.; Benfatto, L.; Cappelluti, E.; Crassee, I.; van der Marel, D.; Blake, P.; Novoselov, K. S.; Geim, A. K. Gate Tunable Infrared Phonon Anomalies in Bilayer Graphene. *Phys. Rev. Lett.* **2009**, *103*, 116804.

(43) Rice, M. J.; Choi, H.-Y. Charged-phonon absorption in doped C_{60}. *Phys. Rev. B: Condens. Matter Mater. Phys.* **1992**, *45*, 10173–10176.

(44) Fu, K.-J.; Karney, W. L.; Chapman, O. L.; Huang, S.-M.; Kaner, R. B.; Diederich, F.; Holczer, K.; Whetten, R. L. Giant vibrational resonances in A_6C_{60} compounds. *Phys. Rev. B: Condens. Matter Mater. Phys.* **1992**, *46*, 1937–1940.

(45) Tanner, D. B.; Jacobsen, C. S.; Bright, A. A.; Heeger, A. J. Infrared studies of the energy gap and electron-phonon interaction in potassium-tetracyanoquinodimethane (K-TCNQ). *Phys. Rev. B* **1977**, *16*, 3283–3290.

(46) Rice, M. J.; Lipari, N. O.; Strässler, S. Dimerized Organic Linear-Chain Conductors and the Unambiguous Experimental Determination of Electron-Molecular-Vibration Coupling Constants. *Phys. Rev. Lett.* **1977**, *39*, 1359–1362.

(47) Khatkale, M. S.; Devlin, J. P. The vibrational and electronic spectra of the mono-, di-, and trianon salts of TCNQ. *J. Chem. Phys.* **1979**, *70*, 1851–1859.

(48) Damascelli, A.; Schulte, K.; van der Marel, D.; Menovsky, A. A. Infrared spectroscopic study of phonons coupled to charge excitations in FeSi. *Phys. Rev. B: Condens. Matter Mater. Phys.* **1997**, *55*, R4863–R4866.

(49) Tanigaki, K.; Ebbesen, T. W.; Saito, S.; Mizuki, J.; Tsai, J. S.; Kubo, Y.; Kuroshima, S. Superconductivity at 33 K in CsxRbyC60. *Nature* **1991**, *352*, 222.

(50) Gunnarsson, O. Superconductivity in fullerides. *Rev. Mod. Phys.* **1997**, *69*, 575–606.

(51) Jérome, D. Organic Conductors: From Charge Density Wave TTF-TCNQ to Superconducting (TMTSF)2PF6. *Chem. Rev.* **2004**, *104*, 5565–5592.

(52) Cao, Y.; Fatemi, V.; Fang, S.; Watanabe, K.; Taniguchi, T.; Kaxiras, E.; Jarillo-Herrero, P. Unconventional superconductivity in magic-angle graphene superlattices. *Nature* **2018**, *556*, 43.

(53) Wu, F.; MacDonald, A. H.; Martin, I. Theory of Phonon-Mediated Superconductivity in Twisted Bilayer Graphene. *Phys. Rev. Lett.* **2018**, *121*, 257001.

(54) De Liberato, S.; Ciuti, C. Quantum theory of intersubband polarons. *Phys. Rev. B: Condens. Matter Mater. Phys.* **2012**, *85*, 125302.

(55) Mahan, G. D. *Many-Particle Physics*, 2nd ed.; Plenum: New York, NY, 1993.

(56) Matz, R.; Lüth, H. Conduction-Band Surface Plasmons in the Electron-Energy-Loss Spectrum of GaAs(110). *Phys. Rev. Lett.* **1981**, *46*, 500–503.

(57) Jalabert, R.; Das Sarma, S. Quasiparticle properties of a coupled two-dimensional electron-phonon system. *Phys. Rev. B: Condens. Matter Mater. Phys.* **1989**, *40*, 9723–9737.

(58) Hwang, E. H.; Sensarma, R.; Das Sarma, S. Plasmon-phonon coupling in graphene. *Phys. Rev. B: Condens. Matter Mater. Phys.* **2010**, *82*, 195406.

negative refraction of highly squeezed plasmon and phonon polaritons in graphene-boron nitride heterostructures. *Proc. Natl. Acad. Sci. U. S. A.* **2017**, *114*, 6717–6721.

(59) Bezares, F. J.; et al. Intrinsic Plasmon-Phonon Interactions in Highly Doped Graphene: A Near-Field Imaging Study. *Nano Lett.* **2017**, *17*, 5908−5913.

(60) Todorov, Y. Dipolar quantum electrodynamics theory of the three-dimensional electron gas. *Phys. Rev. B: Condens. Matter Mater. Phys.* **2014**, *89*, No. 075115.

(61) Babiker, M.; Loudon, R. Derivation of the Power-Zienau-Woolley Hamiltonian in quantum electrodynamics by gauge transformation. *Proc. R. Soc. London, Ser. A* **1983**, *385*, 439−460.

(62) Hagenmüller, D.; Schachenmayer, J.; Genet, C.; Ebbesen, T.; Pupillo, G. Supplemental Material for "Enhancement of the electron-phonon scattering induced by intrinsic surface plasmon-phonon polaritons *ACS Photonics* **2019**, DOI: 10.1021/acsphotonics.9b00268.

(63) Devos, A.; Lannoo, M. Electron-phonon coupling for aromatic molecular crystals: Possible consequences for their superconductivity. *Phys. Rev. B: Condens. Matter Mater. Phys.* **1998**, *58*, 8236−8239.

(64) Engelsberg, S.; Schrieffer, J. R. Coupled Electron-Phonon System. *Phys. Rev.* **1963**, *131*, 993−1008.

(65) Razado-Colambo, I.; Avila, J.; Vignaud, D.; Godey, S.; Wallart, X.; Woodruff, D. P.; Asensio, M. C. Structural determination of bilayer graphene on SiC(0001) using synchrotron radiation photoelectron diffraction. *Sci. Rep.* **2018**, *8*, 10190.